

## Article

# Mechanical Analysis of Palm-Fiber-Reinforced Sand through Triaxial Tests

Yuxiao Tang <sup>1</sup>, Shaowei Wei <sup>2,3</sup>, Xueyan Liu <sup>1,\*</sup> , Wen Liu <sup>1</sup> and Teng Liu <sup>4</sup>

<sup>1</sup> Department of Civil Engineering, School of Water and Soil Conservation, Beijing Forestry University, Beijing 100083, China

<sup>2</sup> China Academy of Railway Sciences, Institute of Railway Architecture, Beijing 100081, China

<sup>3</sup> Beijing Tieke Special Engineering Technology Co., Ltd., Beijing 100081, China

<sup>4</sup> Beijing Municipal Construction Co., Ltd., Beijing 100079, China

\* Correspondence: xyliu@bjfu.edu.cn

**Abstract:** Triaxial tests were employed to investigate palm-fiber-reinforced sand under consolidated drained conditions in this study. Sixteen series of triaxial tests were carried out to investigate the properties of palm-fiber-reinforced sand. One series of pure sand was also employed for comparison. The deviator stress, stress path, shear strength, volume change, void ratio, and enhanced coefficient of fiber-reinforced sand were studied with different fiber lengths varying from 8 mm to 20 mm and fiber contents varying in mass from 0.3% to 0.9%. The test results indicate that palm fibers were beneficial for enhancing the shear strength of the sand. Compared to the peak shear strength increase of about 10% to 20%, the critical shear strength increased much more, by a little over 100%. Therefore, the fibers played a key role in enhancing the critical shear strength of the sand but not the peak shear strength of the sand. The addition of fiber to sand resulted in prolongation of the axial strain required to reach the critical void ratio and improved the sand's ability to resist larger deformations, enhancing its toughness. Furthermore, the critical shear strength of the sand was positively correlated with both fiber content and fiber length, and the axial strain required to reach the critical shear strength increased with increasing fiber content and length. This study provides valuable experimental data and serves as a reference for temporary reinforcement in geotechnical engineering.

**Keywords:** palm fiber; fiber-reinforced sand; stress path; volume change; shear strength



check for updates

**Citation:** Tang, Y.; Wei, S.; Liu, X.; Liu, W.; Liu, T. Mechanical Analysis of Palm-Fiber-Reinforced Sand through Triaxial Tests. *Sustainability* **2023**, *15*, 5461. <https://doi.org/10.3390/su15065461>

Academic Editor: Constantin Chalioris

Received: 16 January 2023

Revised: 1 March 2023

Accepted: 14 March 2023

Published: 20 March 2023



**Copyright:** © 2023 by the authors. Licensee MDPI, Basel, Switzerland. This article is an open access article distributed under the terms and conditions of the Creative Commons Attribution (CC BY) license (<https://creativecommons.org/licenses/by/4.0/>).

## 1. Introduction

Fiber reinforcement technology is an effective measure for soil and water conservation, as it can enhance the mechanical properties of soil and improve its structure. Consequently, this technology is commonly used in road and slope protection projects [1–4]. In China, the rapid development of urban subways and utility tunnels in cities located near rivers with widely distributed sand layers poses a significant engineering challenge. During the tunneling process, liquefaction, collapse, instability, and erosion can occur in the sand aquifer, leading to uneven settlement or ground collapse, which can be detrimental to the project. To overcome this challenge, fiber-reinforced technology is employed to enhance the stability of sand-bearing aquifers during tunnel boring.

In recent years, researchers have investigated the effects of various fibers on the shear strength of sand [5–9]. They have analyzed the impact of factors such as grain size [10], moisture content [10–12], relative density [13], fiber aspect ratio [14], fiber content [15–17], fiber distribution orientation [18–21], and stress paths [22] using triaxial tests or direct shear tests [23,24]. The results of these tests have indicated that higher compactness leads to a larger shear modulus in sand with fibers. Additionally, increased fiber content continuously strengthens the liquefaction resistance and shear modulus of sand samples [25]. Randomly distributed fibers were also found to be more effective in improving the shear strength of dry sand [15]. Moreover, the shear dilatancy of fiber-reinforced sand has been investigated

in relation to deviator stress, and the results have shown that inflation failure occurs more prominently in fiber-reinforced sand than in pure sand [26–28], indicating that sand mixed with fibers has a higher shear strength.

Various types of fibers are available, including carbon fiber, glass fiber, nylon fiber, steel fiber, and plant fiber. Of these, plant fibers such as jute fiber, coir fiber, sisal fiber, flax fiber, straw fiber, and palm fiber have the significant advantage of being eco-friendly. Previous research showed that coir mat reinforcement significantly improved the behavior of sand foundations [29]. The inclusion of coir mat reinforcement redistributed the applied footing load to a more uniform pattern, resulting in reduced settlement [20]. Discrete coir fibers in a random distribution were also found to improve the shear strength of clay significantly [30]. Similarly, sisal fibers in a random distribution were identified as a good reinforcement material for soil [31]. In addition, plant roots can prevent the limited flow failure of soil at cyclic stress ratios, while liquefaction resistance increases with an increase in the root content [32]. As a result, roots mainly improve the cohesion of soil [33]. Researchers proposed a new generalized three-dimensional anisotropic failure criterion for rooted soils based on the results of tests that used the projection of two independent microstructure fabric tensors on the stress tensor [33].

Reinforced concrete, both metallic and non-metallic, is a common structural material used in construction and engineering projects, such as bridges. It involves increasing the strength and toughness of concrete by adding steel reinforcements or other metallic materials [34,35]. However, in addition to metallic materials, there is another material that can be used to reinforce concrete, which is plant fiber. Extensive research has been carried out on plant fiber-reinforced concrete (PFRC) by scholars both domestically and internationally. It has been found that adding short plant fibers to concrete inhibits the development of diagonal cracks by transferring the tensile stress across the crack surface. This transfer capability is commonly referred to as crack bridging [36]. Additionally, the bonding action between the fibers and the mortar provides significant shear resistance to developing cracks [37]. As a result, PFRC exhibits a pseudo-ductile response relative to the brittle behavior of conventional concrete mixtures [38]. PFRC also has higher compressive, splitting tensile, and flexural strengths than conventional concrete [39–42]. The beneficial properties of plant fibers in tension are important for the shear response of concrete members. Therefore, they are an ideal material for enhancing the shear performance of concrete members.

Despite the apparent benefits of plant fibers in enhancing the strength and durability of concrete, there is still much to be learned about their use in geotechnical engineering. For example, there is little current research on the residual resistance during the shearing of fiber-reinforced sand as an expanded frame for PFRC. Moreover, the effect of different ratios of palm fiber on the volume change and void ratio during the shearing of reinforced sand is not entirely clear. Therefore, the study of parameters such as fiber aspect ratio and fiber content is critical for the design of temporary reinforcements for water-rich sandy structures in geotechnical engineering. This research also provides valuable insights for the practical applications of plant fiber-reinforced concrete.

In light of these factors, the authors of the study investigated palm-fiber-reinforced sand with triaxial tests under consolidated drained conditions. Sixteen series of palm-fiber-reinforced sand samples were tested, while one series of pure sand samples was also tested for comparison. The analysis of these results sheds light on the enhancing effects of fiber length and content on the shear strength and strain, void ratio, and volume variation of sand samples.

## 2. Materials and Test Setup

### 2.1. Materials

As shown in Figure 1, the sand tested in this study was quartz sand from Zhengzhou, China. Its physical parameters are shown in Table 1. The palm fibers, with diameters of 0.2 mm to 0.5 mm, were produced in Malaysia. Their tension strength was between 90 kPa

and 220 kPa, with a Young's modulus of 0.45~1.1 GPa. The break elongation was about 15%~25%. In the tests, the palm fibers were cut into lengths of 8 mm, 12 mm, 16 mm, and 20 mm in order to analyze the aspect ratio effects, as shown in Figure 2.



Figure 1. Quartz sand employed in this study (unit: cm).

Table 1. Physical parameters of quartz sand.

Specific Gravity of Soil Particle	Coefficient of Uniformity	Coefficient of Curvature	Maximum Unit Weight (kN/m <sup>3</sup> )	Minimum Unit Weight (kN/m <sup>3</sup> )	Maximum Void Ratio	Minimum Void Ratio
2.65	2.36	1.08	16.10	12.50	1.12	0.64

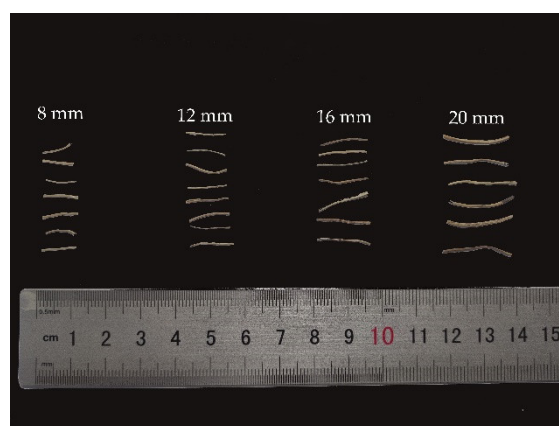
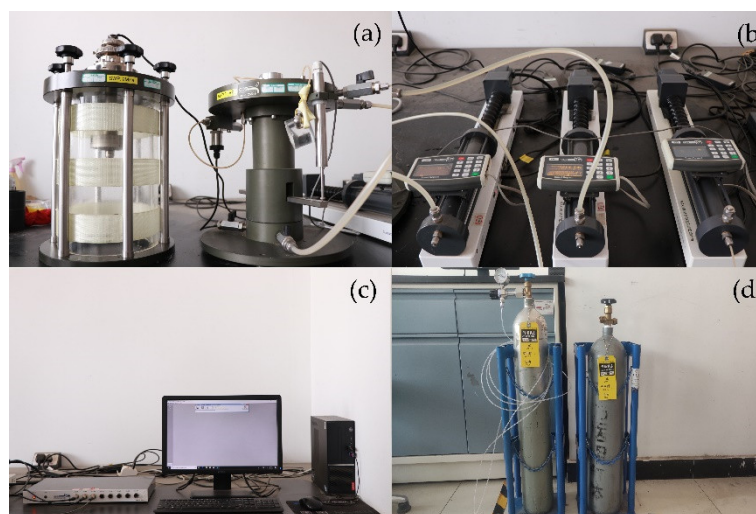


Figure 2. Palm fiber employed in this study (unit: mm).

## 2.2. Test Setup

Triaxial compressive tests on the sand samples under consolidated drained conditions were carried out with a triaxial test apparatus from Global Digital Systems Ltd. (GDS, Hook, UK), as shown in Figure 3. There were four components in the triaxial test system, specifically the pressure chamber, pressure controller, information acquisition equipment, and carbon dioxide cylinder. The sample was a standard cylinder with a size of 100 mm (height)  $\times$  50 mm (diameter). The density of the sand sample was about 1490 kg/m<sup>3</sup> with a void ratio of 0.78, resulting in a relative density of 72%, according to the parameters shown in Table 1. Sixteen series of triaxial tests were performed on the fiber-reinforced sand samples, and one series of triaxial tests was carried out on the pure sand samples for comparison, as shown in Table 2. The tests were carried out according to the China Specification for Highway Geotechnical Test (JTC3430-2020), and the specific steps are shown in Figure 4.



**Figure 3.** The triaxial test apparatus from GDS located at the Beijing Forestry University. (a) The pressure chamber; (b) the pressure controller; (c) the information acquisition equipment; (d) the carbon dioxide cylinder.

**Table 2.** Sample conditions for triaxial tests.

No.	Fiber Length (mm)	Fiber Content (%)	Confining Pressure (kPa)
1	8	0.3	100, 200, 400
2		0.5	100, 200, 400
3		0.7	100, 200, 400
4		0.9	100, 200, 400
5	12	0.3	100, 200, 400
6		0.5	100, 200, 400
7		0.7	100, 200, 400
8		0.9	100, 200, 400
9	16	0.3	100, 200, 400
10		0.5	100, 200, 400
11		0.7	100, 200, 400
12		0.9	100, 200, 400
13	20	0.3	100, 200, 400
14		0.5	100, 200, 400
15		0.7	100, 200, 400
16		0.9	100, 200, 400
17	—	—	100, 200, 400

(1) Palm fibers were added to the sand sample and then mixed until a random and uniform distribution was achieved, as shown in Figure 5, five layers of the sample were prepared, and each layer was compacted;

(2) A carbon dioxide depletion method was employed with the following steps: The gas cylinder filled with carbon dioxide was connected to the valve for the pore pressure. The Perspex cylinder was filled with water, and 20 kPa of confining pressure was applied to the sample. The valves for the pore pressure and back pressure were opened, and carbon dioxide was released into the sample. Note that the pressure of carbon dioxide should not be larger than 20 kPa. This procedure lasted for about 1 h;

(3) Then, a hydrostatic pressure depletion method was utilized with the following steps: 10 kPa of pressure was applied through the valve for the back pressure, and the water was flushed from the bottom of the sample. The flushed water drove out the air in the sample until the volumes of water flushing in and out were equal to each other. The valve for the back pressure was turned off after about 2 h of water flushing;

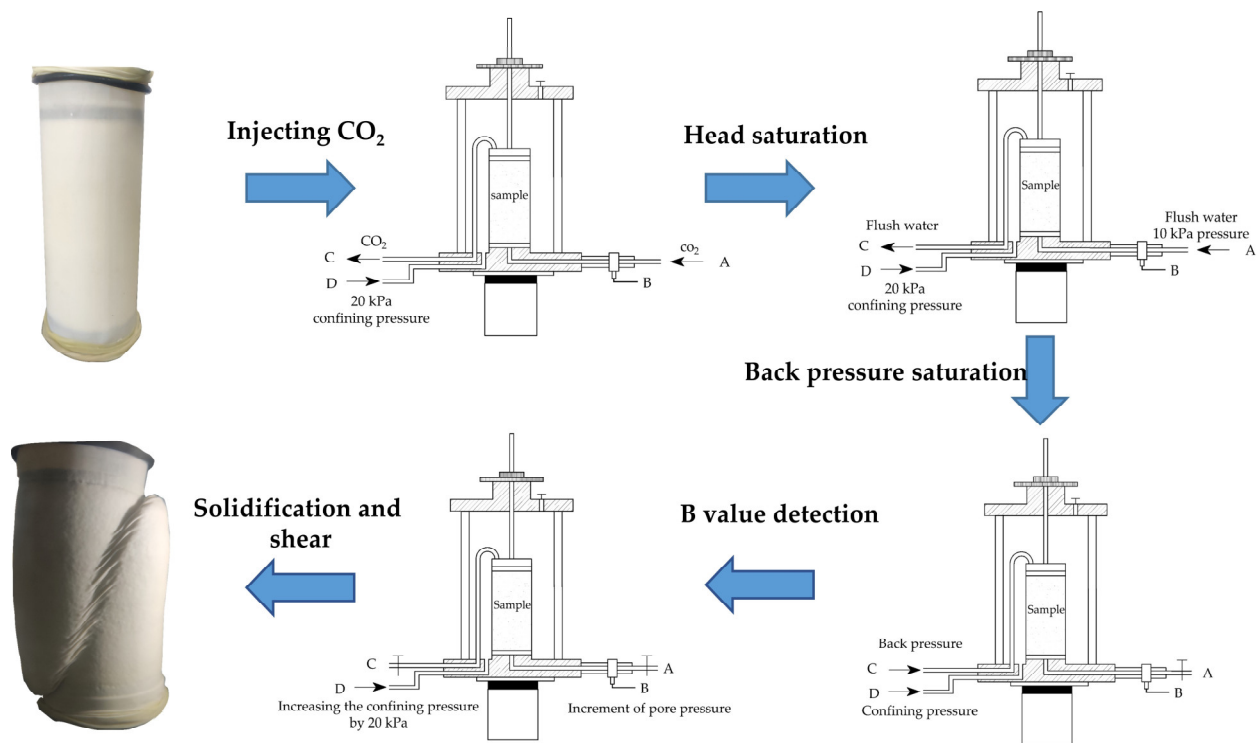


**Figure 4.** Schematic of the test procedure. (A) Pore pressure valve, connected to the bottom of the specimen; (B) pore pressure sensor; (C) back pressure valve, connected to the top of the specimen; (D) circumferential pressure valve.

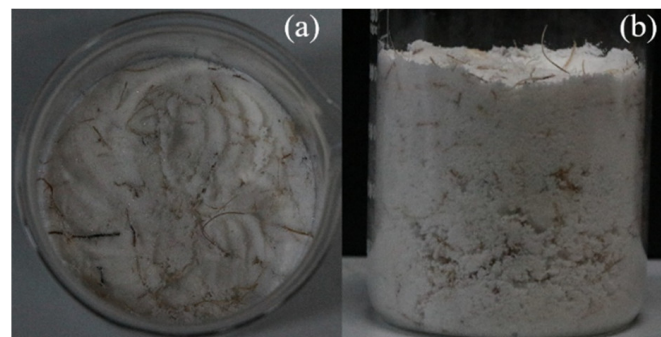


**Figure 5.** Sand mixed with randomly and uniformly distributed palm fibers: (a) top view and (b) front view.

(4) Then, a back pressure saturation method was employed. The confining pressure and back pressure were increased by 30 kPa every 0.5 h. However, initially and throughout the process, the back pressure was 20 kPa lower than the confining pressure;

(5) The B value was tested after 1 h or more and is defined as the increment of pore pressure divided by the increment of confining pressure. The saturation was identified when the B value was larger than 0.95 but smaller than 1.0;

(6) Consolidation was carried out with the confining pressure set as required. The process ended when the back volume maintained a constant volume for 2 s. Then, the shear process was carried out at a speed of 1% of the height per second until the axial strain reached 20%.

### 3. Test Results

#### 3.1. Deviator Stress and Strain

The deviator stress varied with the axial strain in different samples under confining pressures of 100 kPa, 200 kPa, and 400 kPa, as shown in Figure 6a–c. At 100 kPa of confining pressure, the deviator stress obtained larger peak and critical values for the fiber-reinforced sand than for the pure sand, as shown in Figure 6a. The deviator stress also obtained larger values for the fiber-reinforced sand than for the pure sand at confining pressures of 200 kPa and 400 kPa, though the strengthening effect was much lower than that with 100 kPa of confining pressure. For example, with 100 kPa of confining pressure and a fiber length of 20 mm, the critical and peak values of the deviator stress increased by 31.4% and 118.5%, respectively, for the fiber-reinforced sand compared to the pure sand, while under 400 kPa of confining pressure, the peak and critical values of the deviator stress for the fiber-reinforced sand with the same fiber length increased by 18.3% and 48.4%, respectively. The deviator stress almost increased with increases in fiber length. However, under higher confining pressure, the gap between the deviator stresses of the reinforced sand and the pure sand became smaller. Note that the deviator stress was an average value for one fiber length with different fiber contents. For example, the deviator stress of the 8 mm fiber-reinforced sand was the average of the 8 mm fiber-reinforced sand samples with fiber contents of 0.3%, 0.5%, 0.7%, and 0.9%, and the same applies to the values for fiber-reinforced sand with different fiber contents, as shown in Figure 7a–c. With different fiber contents, fiber-reinforced sand also showed obviously increased deviator stresses from the pure sand.

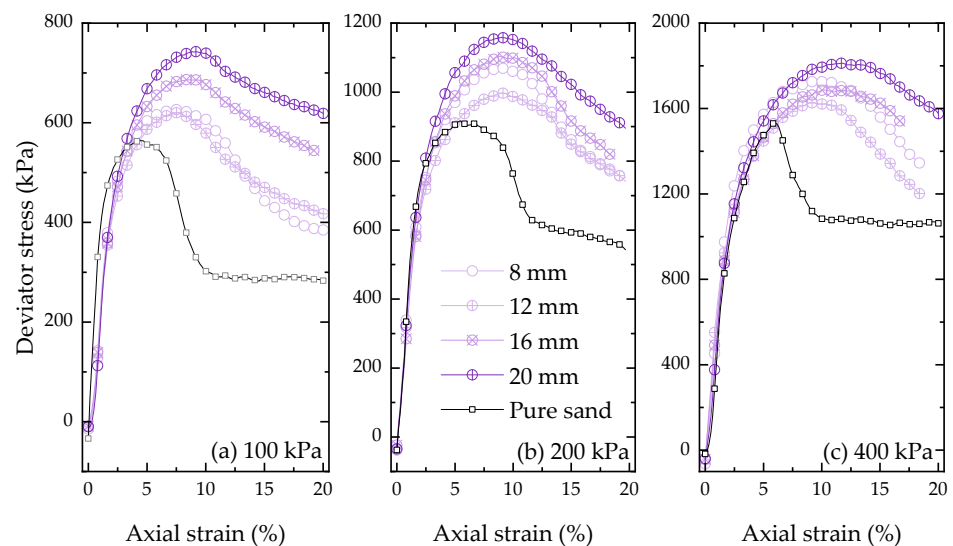


**Figure 6.** Deviator stress with axial strain of sand with different fiber lengths under three confining pressures.

With 100 kPa of confining pressure, the deviator stress of the fiber-reinforced sand increased with the fiber content, as shown in Figure 7a. However, the differences in the deviator stress among the different fiber contents became smaller with increased confining pressure, as shown in Figure 7a–c. Based on the relationships between the deviator stress and axial strain shown in Figure 8, at an axial strain of 4%, the pure sand reached its peak value of deviator stress, while at an axial strain of 15%, the fiber-reinforced sand reached its peak value of deviator stress. The peak deviator stress of the fiber-reinforced sand increased but was reached later than that of the pure sand, indicating that the deviator stress of the fiber-reinforced sand increased due to the palm fibers. Simultaneously, the critical value of the shear strength also increased for the fiber-reinforced sand. Therefore, the strain-softening behavior of the pure sand became strain-hardening behavior in the fiber-reinforced sand, which had a better ability to resist deformation.

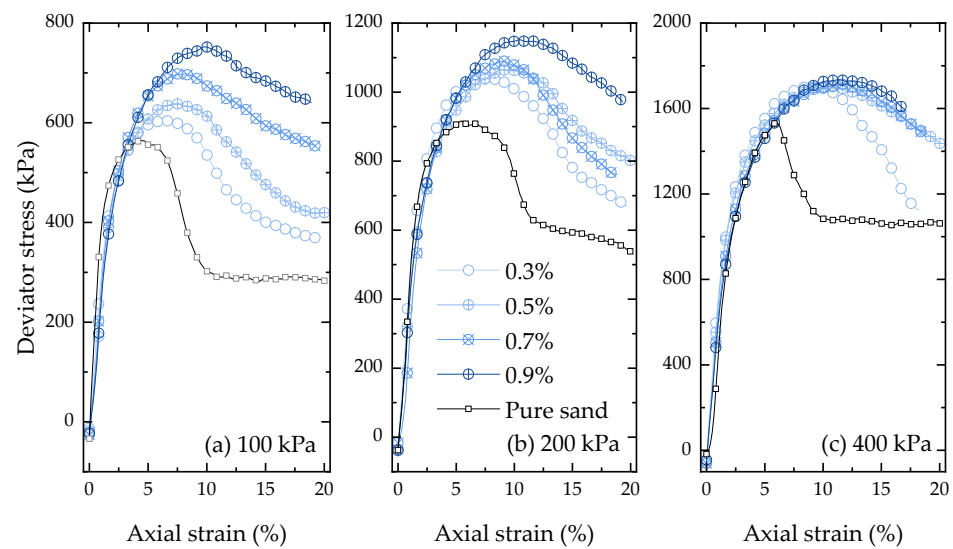


**Figure 7.** Deviator stress with axial strain of sand with different fiber contents under three confining pressures.

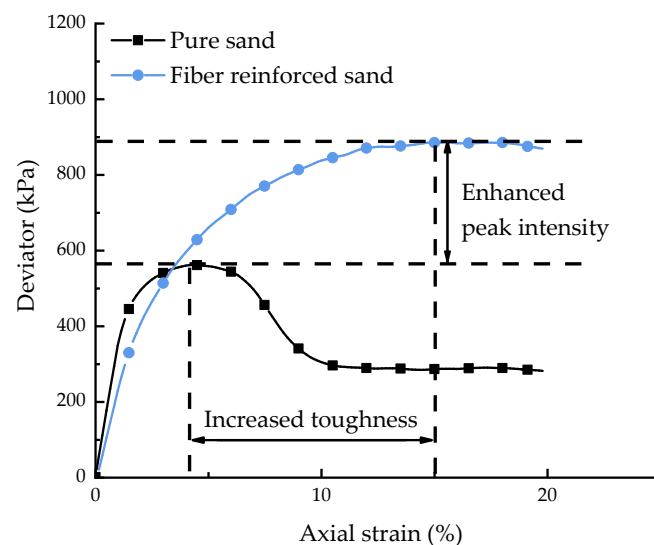


**Figure 8.** Deviator stress with axial strain of fiber-reinforced sand and pure sand.

### 3.2. Stress Path

Figure 9 shows that the stress path varied with the different confining pressures and fiber lengths using the  $p'$ - $q$  system.  $p'$  is the mean effective stress and  $q$  is the peak deviatoric stress. The maximum values of  $p'$  and  $q$  indicate the peak values of the shear strength, while the minimum values of  $p'$  and  $q$  suggest the critical values of the shear strength. The confining pressures of 100 kPa, 200 kPa, and 400 kPa are depicted in the same figure, forming the failure lines of the peak shear failure and critical shear failure, as shown in Figure 9a. The peak shear failure lines were obtained through linear regression of the three peak shear failure points. The critical shear failure lines were obtained through linear regression of the three critical shear failure points. The enhancement in the overall strength of the specimen is reflected in the movement of the peak and critical shear failure lines. As shown in Figure 9a–e, compared to the failure lines of pure sand, the failure lines of the fiber-reinforced sand obtained higher values and bigger slope gradients, and the critical failure lines are closer to the corresponding peak failure lines. Therefore, the critical shear strength of the fiber-reinforced sand increased. Moreover, in comparison to pure sand, the critical failure lines of the fiber-reinforced sand increased more than their peak failure lines.

Thus, the palm fibers enhanced the critical shear strength more obviously than the peak shear strength in fiber-reinforced sand.

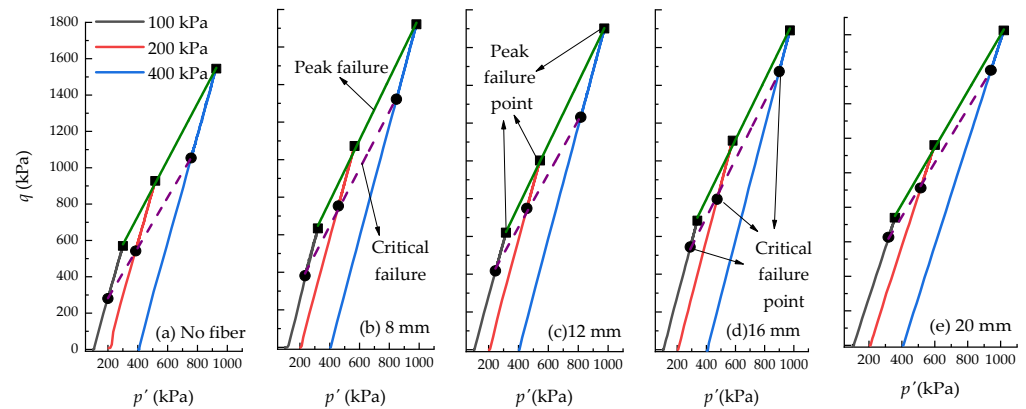


Figure 9. Stress paths with different confining pressures and fiber lengths.

Figure 10 shows that the stress path varied with different confining pressures and fiber contents in the  $p'$ - $q$  system. Compared to the pure sand, the peak and critical failure values of the fiber-reinforced sand were higher. Moreover, the critical failure values of the fiber-reinforced sand obviously increased and became closer to the peak failure values with increases in the fiber content, as shown in Figure 10c–e.

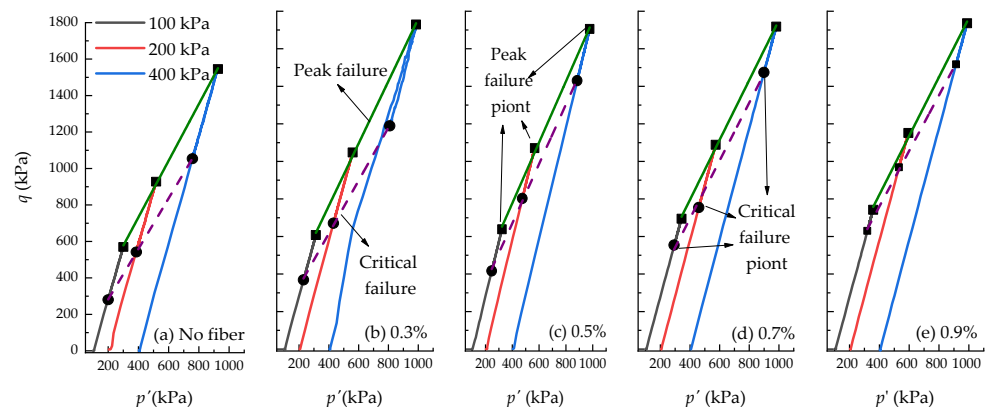


Figure 10. Stress paths with different confining pressures and fiber contents.

### 3.3. Shear Strength

The intensity envelopes of effective stress at 100 kPa, 200 kPa, and 400 kPa of confining pressure for the pure sand are depicted in Figure 11 using the  $\tau$ - $\sigma$  system. The intensity envelopes became weaker with increases in the confining pressure. A linear intensity envelope with a large intercept was obtained via linear regression, leading to a large value of cohesion, which is not common for sand. In fact, the sand particles were destroyed under high pressure, indicating weak shear strength. The slopes of intensity envelopes for different confining pressures were calculated separately, and then their average value was employed for further analysis. The shear strengths of the fiber-reinforced sand and pure sand were calculated using Equation (1). The shear strength parameters of each sample obtained with the averaging method are listed in Table 3. It can be seen that the friction angle of the fiber-reinforced sand was larger than that of the pure sand. Therefore, the palm fibers distributed in the sand had a strong reinforcing effect, which is also presented in Figure 12. This shows that the friction angle of the sand samples generally increased with fiber content for the same fiber length, and generally increased with the fiber length, except for the fiber length of 8 mm.

$$\tau = \sigma \tan \varphi + c \quad (1)$$

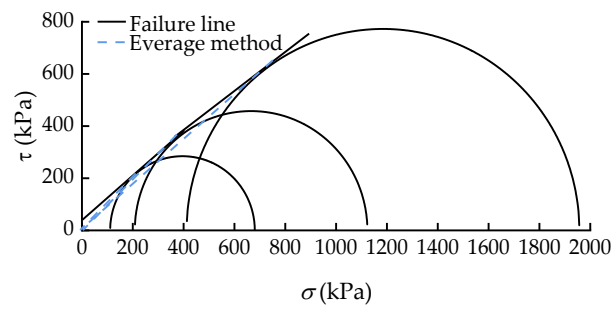


Figure 11. Mohr–Coulomb failure circles and intensity envelopes of pure sand.

Table 3. Strength parameters of fiber-reinforced sand.

Fiber Length (mm)	Fiber Content (%)	$(\sigma_1 - \sigma_3)_f$ (kPa)			$c$ (kPa)	$\varphi$ (°)	
		100 kPa	200 kPa	400 kPa			
0	0	465	927	1545	0	43.3	
	8	0.3	614	1071	1816	0	46.5
		0.5	587	1093	1722	0	46.1
		0.7	699	1120	1772	0	47.3
		0.9	672	1072	1680	0	46.5
12	0.3	551	905	1669	0	44.5	
	0.5	602	997	1668	0	45.5	
	0.7	612	957	1595	0	45.1	
	0.9	757	1156	1711	0	47.6	
16	0.3	640	1042	1650	0	46.0	
	0.5	658	1092	1721	0	46.6	
	0.7	733	1133	1722	0	47.4	
	0.9	822	1227	1735	0	48.4	
20	0.3	652	1191	1795	0	47.3	
	0.5	724	1130	1788	0	47.5	
	0.7	811	1204	1914	0	48.8	
	0.9	889	1236	1901	0	49.3	

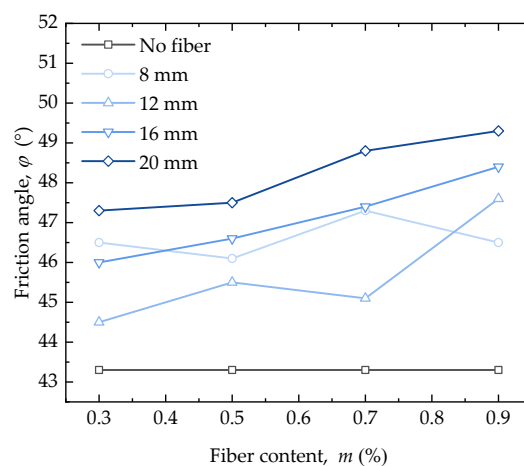


Figure 12. Series of friction angles with different fiber contents.

### 4. Discussion

#### 4.1. Volume Change

Figure 13 shows volume changes with axial strain in the pure sand and palm-fiber-reinforced sand with different fiber lengths. The volume of the pure sand initially decreased with 1% axial strain but then increased to a stable value, as shown in Figure 13a–c. The

ultimate values of the volume changes of pure sand under confining pressures of 100 kPa, 200 kPa, and 400 kPa were 5.38%, 2.98%, and 1.05%, respectively. The volumes of the fiber-reinforced sand had a trend similar to that of the pure sand, but they reached higher values and kept increasing rather than converging on a stable value. When the axial strain reached 20%, the volume change of the fiber-reinforced sand still had an increasing trend. The increase in volume means that dilatancy occurred in the sand. Therefore, dilatancy continuously occurred for the fiber-reinforced sand, which was different from the pure sand. On the other hand, when the confining pressure increased from 100 kPa to 200 kPa and then to 400 kPa, the volume increased by smaller and smaller values, as shown in Figure 13a–c. With 100 kPa of confining pressure, the final values of volume change (axial shear strain of 20%) corresponding to the different fiber lengths were 6.12% at 8 mm, 6.35% at 12 mm, 7.17% at 16 mm, and 7.81% at 20 mm. At 200 kPa of confining pressure, the final values of volume change (axial shear strain of 20%) for the different fiber lengths were 4.96% at 8 mm, 5.59% at 12 mm, 5.76% at 16 mm, and 5.92% at 20 mm. At 400 kPa of confining pressure, the final values of volume change (axial shear strain of 20%) corresponding to the different fiber lengths were 3.04% at 8 mm, 3.28% at 12 mm, 3.32% at 16 mm, and 3.69% at 20 mm. Therefore, dilation was not as obvious for high confining pressure as it was for low confining pressure, although the fiber-reinforced sand had similar trends under different confining pressures. Above all, dilatancy was more obvious for longer fiber-reinforced sand under lower confining pressure.

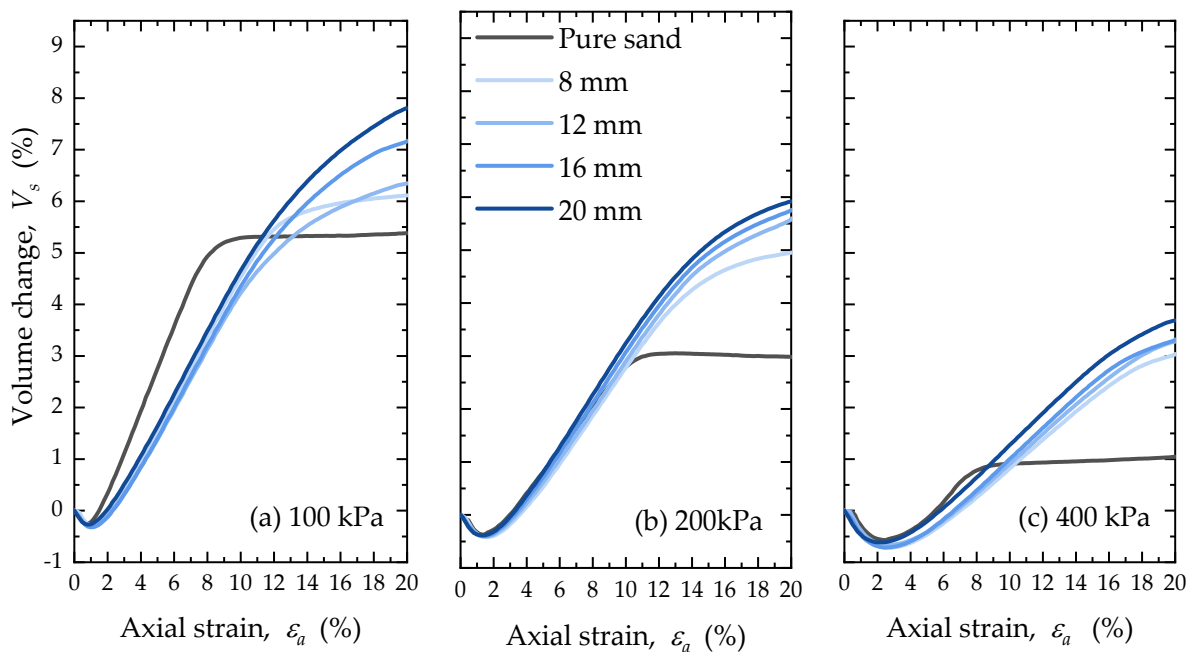


**Figure 13.** Volume changes with different axial strain and fiber lengths.

Figure 14 shows volume changes with axial strain for the pure sand and palm-fiber-reinforced sand with different fiber contents. At 100 kPa of confining pressure, the ultimate values of volume change (axial shear strain of 20%) relative to the different fiber contents were 6.68% at 0.3%, 7.06% at 0.5%, 7.15% at 0.7%, and 7.48% at 0.9%. With 200 kPa of confining pressure, the final values of volume change (axial shear strain of 20%) corresponding to the different fiber contents were 5.07% at 0.3%, 5.14% at 0.5%, 5.27% at 0.7%, and 5.45% at 0.9%. With 400 kPa of confining pressure, the final values of volume change (axial shear strain of 20%) corresponding to the different fiber contents were 3.04% at 0.3%, 3.30% at 0.5%, 3.32% at 0.7%, and 3.58% at 0.9%. It can be seen that continuous dilatancy also occurred in the fiber-reinforced sand with different fiber contents. However, the volume changes with the axial strain were similar for fiber-reinforced sand with all fiber contents.

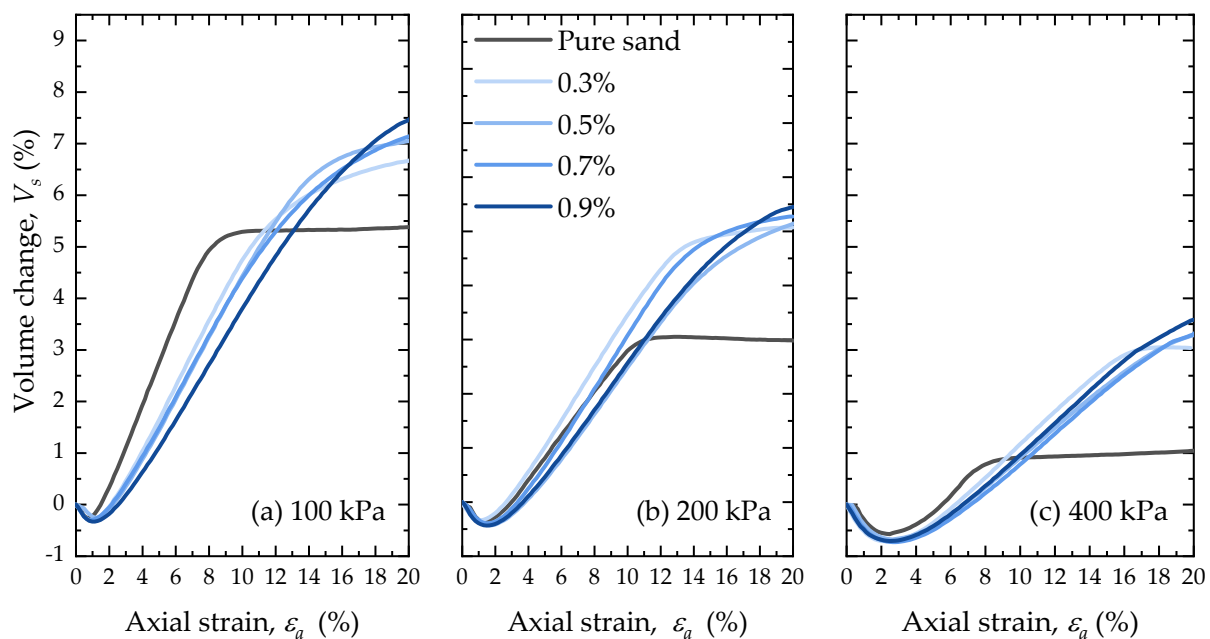


**Figure 14.** Volume changes with different axial strain and fiber contents.

#### 4.2. Void Ratio

Figure 15a shows void ratio changes with axial strain for the test series of the pure sand and fiber-reinforced sand with different fiber lengths. For all samples, there was a small initial decrease in the void ratio, followed by increases to larger and more steady values. The critical void ratios of the pure sand samples under confining pressures of 100 kPa, 200 kPa, and 400 kPa were 0.86, 0.81, and 0.77, while the initial void ratios of the pure sand samples at 100 kPa, 200 kPa, and 400 kPa of confining pressure were 0.77, 0.76, and 0.75, which shows that the void ratio variation became smaller with increases in the confining pressure. Compared to the pure sand, the void ratios of the fiber-reinforced sand were higher at the residual stage of the shearing process, and the values were commonly higher for longer fiber-reinforced sand. This proves that the palm fibers enhanced the strain resistance of the sand samples.

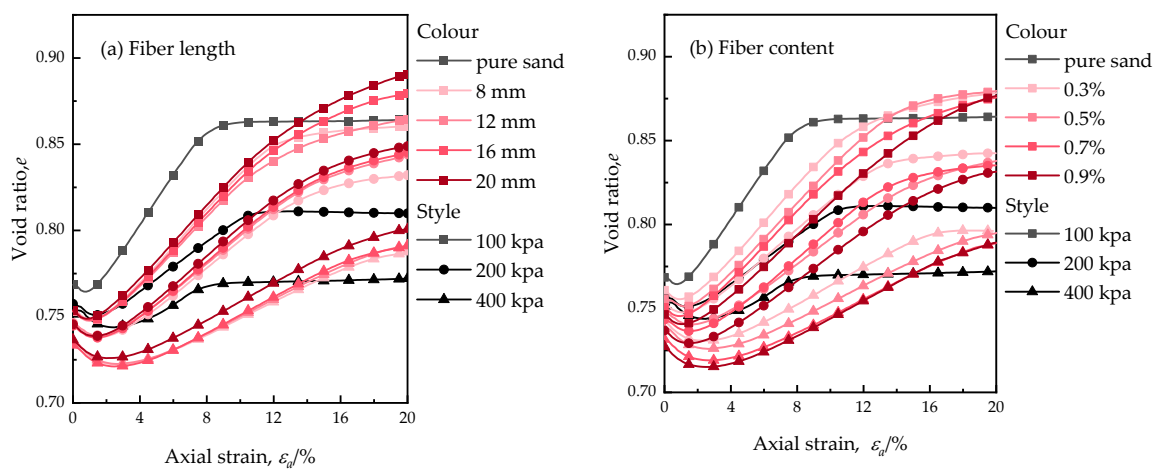


**Figure 15.** Void ratios with axial strain: (a) fiber length and (b) fiber content.

Figure 15b shows void ratio changes with axial strain for the test series of the pure sand and fiber-reinforced sand with different fiber contents. As above, for all samples, there were small initial decreases in the void ratios, and then they increased successively. The void ratios decreased with increases in confining pressure, too, and also increased

at the residual stage from the pure sand to the fiber-reinforced sand. However, the void ratio appeared to decrease with increases in the fiber content, but not obviously. The addition of fibers decreased the initial void ratios of the pure sand. The higher the fiber content, the smaller the initial void ratio, which had the effect of enhancing the void ratios at the residual stage of the shearing process. Based on the relationships between the void ratio and the axial strain shown in Figure 16, the initial void ratio of the reinforced sand was smaller than that of the pure sand due to the addition of fibers. In the dilatancy stage, the void ratio of the fiber-reinforced sand kept rising, while the void ratio of the pure sand reached a critical value at about 10% axial strain. In contrast to Figure 8, the deviator stress at 10% axial strain also reached the residual value. The addition of fibers increased the critical porosity ratio of the sand, and the axial deformation of the specimen to reach the critical state also increased, so the overall strength and toughness of the sand were enhanced.

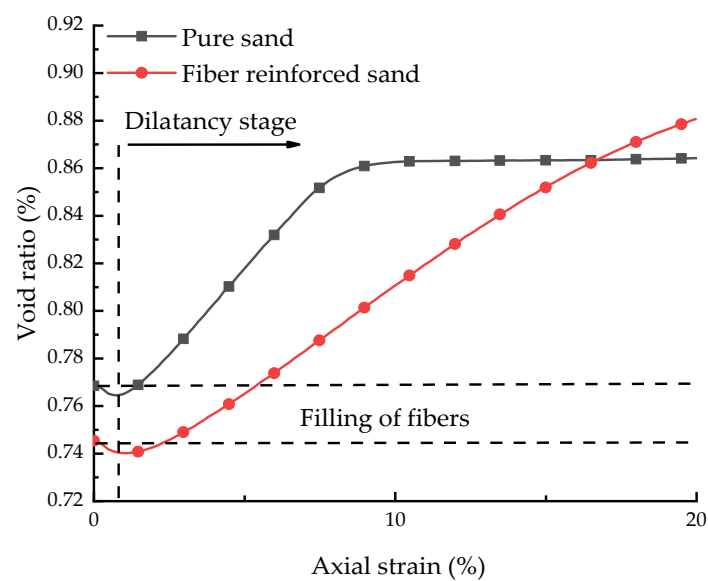


**Figure 16.** Void ratio with axial strain of fiber-reinforced sand and pure sand.

#### 4.3. Enhanced Strength of Fiber-Reinforced Sand

The coefficient of the enhanced strength of the fiber-reinforced sand estimated with deviator stress was calculated using Equation (2) [43], as follows:

$$R_{\sigma} = \frac{(\sigma_1 - \sigma_3)_f^R}{(\sigma_1 - \sigma_3)_f} \quad (2)$$

where  $(\sigma_1 - \sigma_3)_f^R$  is the peak value of the deviator stress of the fiber-reinforced sand, and  $(\sigma_1 - \sigma_3)_f$  is the peak value of the deviator stress of the pure sand.

The reinforcing effects of palm fibers with different lengths and contents on the sand are compared in Figure 17. To better analyze the reinforcement effects of the fibers on the sand, the average strength coefficients of three kinds of confining pressure with the same fiber length or fiber content was taken. For example, the average strength coefficient of 8 mm fiber-reinforced sand is the mean strength coefficient of the 8 mm fiber-reinforced sand samples at 100 kPa, 200 kPa, and 400 kPa. As shown in Figure 16a, the average reinforcement coefficients corresponding to 8 mm, 12 mm, 16 mm, and 20 mm are 1.15, 1.09, 1.19, and 1.28, respectively. Therefore, the coefficient of the reinforcing effect generally increased with fiber length. However, for the same fiber length, the coefficient of the reinforcing effect somewhat decreased with confining pressure. For example, at 20 mm, the strength coefficients corresponding to fiber-reinforced sand samples at 100 kPa, 200 kPa, and 400 kPa are 1.38, 1.26, and 1.20, respectively. Thus, the reinforcing effect was larger

for lower confining pressure. On the other hand, the coefficient of the reinforcing effect increased with fiber content. The average reinforcement coefficients corresponding to the fiber contents of 0.3%, 0.5%, 0.7%, and 0.9% were 1.11, 1.13, 1.20, and 1.26, respectively, as shown in Figure 17b. Similarly, for the same fiber length, the coefficient, in some respects, decreased with confining pressure, especially for higher fiber contents. For example, with a fiber content of 0.9%, the strength coefficients at 100 kPa, 200 kPa, and 400 kPa for the fiber-reinforced sand are 1.39, 1.27, and 1.14, respectively.

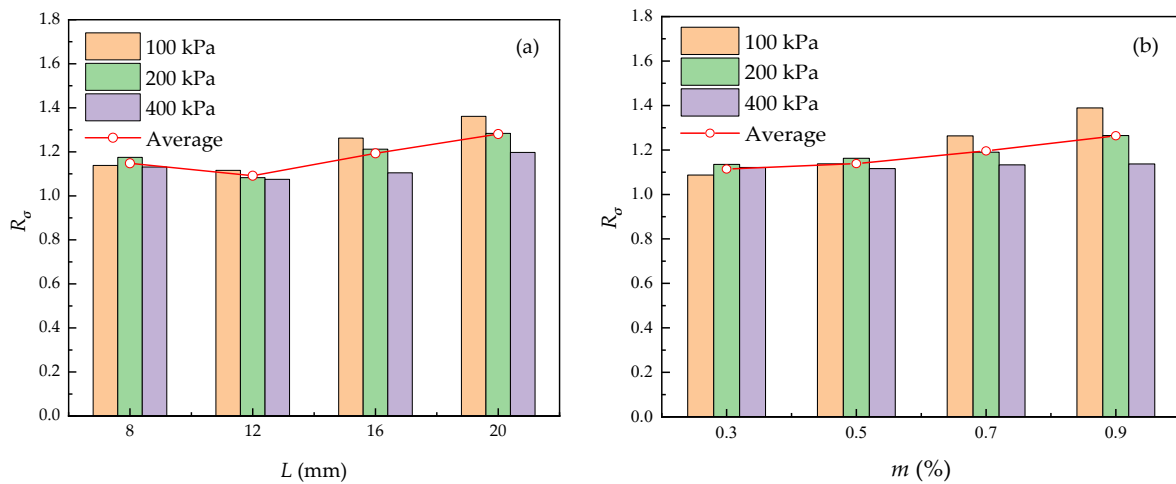


**Figure 17.** Reinforcing effect coefficients: (a) with fiber length and (b) with fiber content.

#### 4.4. Fiber Reinforcement Mechanisms

As shown in Figure 18, the fibers filled the spaces between the sand grains, which reduced the initial void ratio of the pure sand. The fibers acted as a spatial interconnection network between the sand particles, locking sand particles and fibers together. When the fiber-reinforced specimen was sheared, the interaction between the sand particles and the fibers prevented the fibers from coming out, and part of the shear stress was defined by the tensile strength of the fibers. The stress–dilatancy parameter of fiber tensile strength enhancement is  $\sigma_{FR}$  [26]. When the tensile force of the fibers was fully mobilized, the ductility of the specimen was enhanced. The volume change and critical void ratio during shearing increased. The interaction between the quartz sand particles and the fibers was enhanced with increases in the fiber length and fiber content. The interfacial force between the palm fiber and the quartz sand particles achieved a reinforcement effect and enhanced the overall residual strength and toughness of the quartz sand in the critical state.

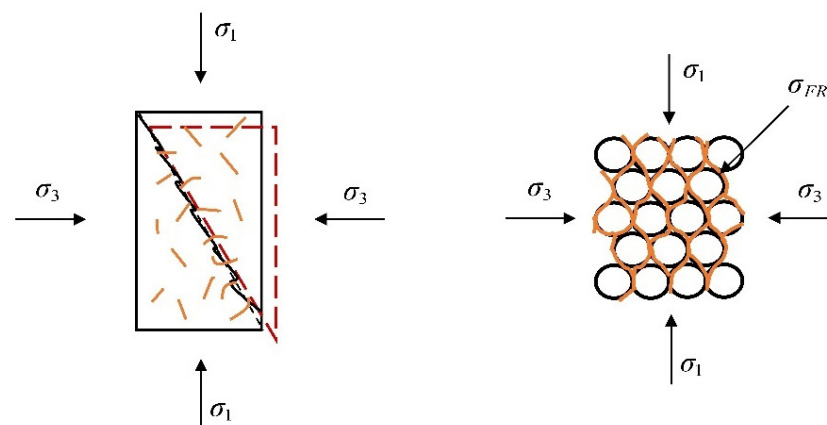


**Figure 18.** Interaction of fibers with quartz sand.

## 5. Conclusions

The deviator stress, stress path, shear strength, volume change, void ratio, and enhanced coefficient of fiber-reinforced sand were analyzed through triaxial compressive tests. The following conclusions can be drawn:

(1) The shear strength of fiber-reinforced sand was higher than that of pure sand, by only about 10% to 20%. However, the critical shear strength of the fiber-reinforced sand increased more than the peak strength, by over 100%. Therefore, the palm fiber played a more obvious role in enhancing the critical shear strength of the sand.

(2) The volume of the fiber-reinforced sand continuously increased with axial strain after initially decreasing, rather than converging to a stable value as that of the pure sand did. The void ratio also increased for the fiber-reinforced sand in comparison to the pure sand. This indicates that the palm fiber increased the strain resistance of the sand with more obvious dilatancy.

(3) The peak shear strength and critical shear strength of the fiber-reinforced sand generally increased with the fiber length and fiber content. However, critical shear strength was associated with fiber content rather than fiber length.

(4) The results show that sand reinforced with longer fibers exhibited more significant shear dilatancy, whereas a higher fiber content did not contribute as much to enhancing the shear dilatancy.

(5) Overall, in-depth analysis of the derived results highlights the positive effects of palm fiber on enhancing critical shear strength and dilatancy in fiber-reinforced sand. These findings can be useful for further research and development in this field.

**Author Contributions:** Conceptualization, Y.T. and X.L.; methodology, Y.T.; analysis, Y.T.; resources, X.L.; writing—original draft preparation, Y.T.; writing—review and editing, Y.T., X.L. and W.L.; supervision, X.L., W.L., S.W. and T.L.; funding acquisition, X.L. All authors have read and agreed to the published version of the manuscript.

**Funding:** The investigation was supported by the National Natural Science Foundation of China (Grant No. 51678037). It was also funded by the Beijing Municipal Construction Co., Ltd. (No. CZDT-02-07-QT-042(KY)).

**Institutional Review Board Statement:** Ethical approval was not required for this study.

**Informed Consent Statement:** No humans were involved in this study.

**Data Availability Statement:** Data available on request due to restrictions eg privacy or ethical. The data presented in this study are available on request from the corresponding author. The data are not publicly available due to confidentiality agreements with research participants.

**Acknowledgments:** The authors are deeply indebted to the financial supporters.

**Conflicts of Interest:** The authors declare no conflict of interest.

## References

1. Bao, X.; Li, L.; Liao, Z.; Cui, H.; Tang, W.; Chen, X. Study of silty sand slope protection from seepage flows using short fiber-sand mixtures. *Geosynth. Int.* **2021**, *28*, 491–507. [[CrossRef](#)]
2. Bao, H.; Liu, C.; Lan, H.; Yan, C.; Li, L.; Zheng, H.; Dong, Z. Time-dependency deterioration of polypropylene fiber reinforced soil and guar gum mixed soil in loess cut-slope protecting. *Eng. Geol.* **2022**, *311*, 106895. [[CrossRef](#)]
3. Lai, T.; Lei, H.; Wu, Z.; Wu, H. Shaking table test study on basalt fiber reinforced plastics in high slope protection. *Rock Soil Mech.* **2021**, *42*, 390–400.
4. Fujiyoshi, K.; Ueda, T.; Takagi, H.; Tsukagoshi, M. Construction Technologies and Architecture. In *Mechanical Properties and Durability of Bamboo Fibers/Bamboo-Fiber-Mixed Spray Mortar for Slope Protection*; Trans Tech Publications: Bäch, Switzerland, 2022; pp. 1–11.
5. Yang, K.H.; Lee, S.; Tsai, M.H.; Nguyen Minh, D.; Wu, C. Behavior of nonwoven-geotextile-reinforced sand and mobilization of reinforcement strain under triaxial compression. *Geosynth. Int.* **2013**, *20*, 207–225.
6. Choobbasti, A.; Soleimani Kutanaei, S.; Ghadakpour, M. Shear behavior of fiber-reinforced sand composite. *Arab. J. Geosci.* **2019**, *12*, 1–6. [[CrossRef](#)]

7. Kong, Y.; Zhou, A.; Shen, F.; Yao, Y. Stress-dilatancy relationship for fiber-reinforced sand and its modeling. *Acta. Geotech.* **2019**, *14*, 1871–1881. [[CrossRef](#)]
8. Yilmaz, Y. Experimental investigation of the strength properties of sand–clay mixtures reinforced with randomly distributed discrete polypropylene fibers. *Geosynth. Int.* **2009**, *16*, 354–363. [[CrossRef](#)]
9. Anagnostopoulos, C.A.; Papaliangas, T.T.; Konstantinidis, D.; Patronis, C. Shear strength of sands reinforced with polypropylene fibers. *Geotech. Geol. Eng.* **2013**, *31*, 401–423. [[CrossRef](#)]
10. Diambra, A.; Ibraim, E. Fibre-reinforced sand: Interaction at the fibre and grain scale. *Géotechnique* **2015**, *65*, 296–308. [[CrossRef](#)]
11. Lovisa, J.; Shukla, S.; Sivakugan, N. Shear strength of randomly distributed moist fiber-reinforced sand. *Geosynth. Int.* **2010**, *17*, 100–106. [[CrossRef](#)]
12. Nozoe, S.; Kasai, Y.; Kaneko, K.; Matsui, K.; Kumagai, K. Relationship between mechanical properties and fiber mixture ratio in fiber-reinforced sand. *Geosynth. Eng. J.* **2012**, *27*, 127–132. [[CrossRef](#)]
13. Tatsuoka, F.; Ishihara, K. Yielding of sand in triaxial compression. *Soils Found.* **1974**, *14*, 63–76. [[CrossRef](#)]
14. Michalowski, R.; Čermaák, J. Triaxial compression of sand reinforced with fibers. *J. Geotech. Geoenviron. Eng.* **2003**, *129*, 125–136. [[CrossRef](#)]
15. Gray, D.; Alrefeai, T. Behavior of Fabric-Versus fiber-reinforced sand. *J. Geotech. Eng.* **1986**, *112*, 804–820. [[CrossRef](#)]
16. Sadek, S.; Najjar, S.; Freiha, F. Shear strength of fiber-reinforced sands. *J. Geotech. Geoenviron. Eng.* **2010**, *136*, 490–499. [[CrossRef](#)]
17. Javdanian, H.; Soltani, N.; Shams, R.; Ghorbani, S. Investigating the monotonic behavior of fiber-reinforced soil under triaxial compression using experimental modeling. *Model. Earth Syst. Environ.* **2021**, *7*, 943–952. [[CrossRef](#)]
18. Michalowski, R.; Čermaák, J. Strength anisotropy of fiber-reinforced sand. *Comput. Geotech.* **2002**, *29*, 279–299. [[CrossRef](#)]
19. Neeraja, V.; Manjari, G.; Babu, G. Numerical analysis of effect of orientation of fibers on stress-strain response of fiber reinforced soil. *Int. J. Geotech. Eng.* **2014**, *8*, 328–334. [[CrossRef](#)]
20. Michalowski, R.L. Limit analysis with anisotropic fibre-reinforced soil. *Geotechnique* **2008**, *58*, 489–501. [[CrossRef](#)]
21. Soriano, I.; Ibraim, E.; Andò, E.; Diambra, A.; Laurencin, T.; Moro, P.; Viggiani, G. 3D fibre architecture of fibre-reinforced sand. *Granul. Matter* **2017**, *19*, 75. [[CrossRef](#)]
22. Chen, C. *Triaxial Compression and Extension Tests for Fiber-Reinforced Silty Sand*; Ground Improvement and Geosynthetics: Shanghai, China, 2010; pp. 367–376.
23. Mali, S. A study on shear strength of sand reinforced with glass fibres. *Int. J. Sci. Eng. Res.* **2013**, *4*, 285–288.
24. Noorzad, R.; Zarinkolaei, S. Comparison of mechanical properties of fiber-reinforced sand under triaxial compression and direct shear. *Open Geosci.* **2015**, *1*, 547–558.
25. Noorzad, R.; Fardad Amini, P. Liquefaction resistance of Babolsar sand reinforced with randomly distributed fibers under cyclic loading. *Soil Dyn. Earthq. Eng.* **2014**, *66*, 281–292. [[CrossRef](#)]
26. Uddin, S.; Marri, A.; Wanatowski, D.; Hall, M. *Stress-Dilatancy and Micromechanics of Fibre-Reinforced Sand*; Geosynthetics ASIA: Bangkok, Thailand, 2012; pp. 683–690.
27. Eldesouky, H.; Morsi, M.; Mansour, M. Fiber-reinforced sand strength and dilation characteristics. *Ain Shams Eng. J.* **2016**, *7*, 517–526. [[CrossRef](#)]
28. Wanatowski, D.; Uddin, S.; Marri, A. *Effects of Discrete Fibers on the Stress-Dilatancy and Micromechanics of Fiber-Reinforced Sand*; Geosynthetics: Long Beach, CA, USA, 2013; pp. 546–554.
29. Rajagopal, S.; Prathap Kumar, M.T. Cyclic response of single-layer coir-mat-reinforced sand. *Innov. Infrastruct. Solut.* **2018**, *3*, 13.
30. Maliakal, T.; Thiyyakkandi, S. Influence of randomly distributed coir fibers on shear strength of clay. *Geotech. Geol. Eng.* **2013**, *31*, 425–433. [[CrossRef](#)]
31. Prabakar, J.; Ramachandran, S.S. Effect of random inclusion of sisal fibre on strength behaviour of soil. *Constr. Build. Mater.* **2002**, *16*, 123–131. [[CrossRef](#)]
32. Karimzadeh, A.; Leung, A.; Hosseinpour, S.; Wu, Z.; Fardad Amini, P. Monotonic and cyclic behaviour of root-reinforced sand. *Can. Geotech. J.* **2021**, *99*, 1915–1927. [[CrossRef](#)]
33. Karimzadeh, A.; Leung, A.; Gao, Z. Shear strength anisotropy of rooted soils. *Géotechnique* **2022**. ahead of print. [[CrossRef](#)]
34. Krishna, B.V.; Rao, D.M.K. A comparative and experimental study on the mechanical properties of various steel and glass fiber reinforced high strength concrete. *IRJET* **2015**, *2*, 129–133.
35. Kroviakov, S.O.; Iu, H.D.; Kryzhanovskiy, V.O.; Zavoloka, M.V.; Yelkin, A.V. Comparison of fiber concrete properties for industrial floors and road pavements with steel and polypropylene fiber. *Build. Mater. Tech.* **2022**, *87*, 76–84. [[CrossRef](#)]
36. Leung, C.K.; Chi, J. Crack-bridging force in random ductile fiber brittle matrix composites. *J. Eng. Mech.* **1995**, *121*, 1315–1324. [[CrossRef](#)]
37. Zhang, J.; Yu, Z.; Sun, X.; Zhang, G.; Pan, W. Experimental study and failure mechanism analysis of rubber fiber concrete under the compression-shear combined action. *Adv. Mater. Sci. Eng.* **2021**, *2021*, 5554257. [[CrossRef](#)]
38. Hu, Q.; Fang, G. Study on Mechanical Properties of Plant Fiber reinforced concrete Hollow Block. *IOP Conf. Ser. Earth Environ. Sci.* **2020**, *446*, 022077. [[CrossRef](#)]
39. Shah, I.; Li, J.; Yang, S.; Zhang, Y.; Anwar, A. Experimental investigation on the mechanical properties of natural fiber reinforced concrete. *J. Renew. Mater.* **2022**, *10*, 1307. [[CrossRef](#)]
40. Gnanasundar, V.M.; Palanisamy, T.S.; Thirugnanam, G.S.; Preetha, V. Mechanical properties of fiber reinforced concrete by using sisal fiber with M-Sand as fine aggregate. *Sustain. Mater. Smart Pract.* **2022**, *23*, 76–82.

41. Vijayalakshmi, R.; Vaishnavi, M.; Geetha, R. Study on the workability, mechanical properties of fish tail palm fibre reinforced concrete-emphasis on fibre content and fibre length. *Eur. J. Environ. Civ. Eng.* **2022**, 1–19. [[CrossRef](#)]
42. Ramalingam, V.; Ramesh, K.; Arumugam, M.; Muralidharan, V. Effect of natural fish tail palm fiber on the workability and mechanical properties of fiber reinforced concrete. *Build. Mater. Struct.* **2022**, *65*, 7–22. [[CrossRef](#)]
43. Xu, W.; Zhang, J.; He, J. Research on large-scale triaxial tests on reinforced soft rock composed of coarse-grained soil as embankment fillings. *Chin. J. Rock Mech. Eng.* **2010**, *29*, 535–541.

**Disclaimer/Publisher’s Note:** The statements, opinions and data contained in all publications are solely those of the individual author(s) and contributor(s) and not of MDPI and/or the editor(s). MDPI and/or the editor(s) disclaim responsibility for any injury to people or property resulting from any ideas, methods, instructions or products referred to in the content.